JHEP

Published for SISSA by Springer

Received: October 24, 2018
Revised: February 8, 2019
Accepted: March 11, 2019
Published: March 22, 2019

Hadron collider sensitivity to fat flavourful Z's for $R_{K^{(*)}}$

B.C. Allanach,[a] **Tyler Corbett,**[1b] **Matthew J. Dolan**[b] **and Tevong You**[a,c]

[a] *DAMTP, University of Cambridge, Wilberforce Road, Cambridge, CB3 0WA, United Kingdom*
[b] *School of Physics, University of Melbourne, Victoria 3010, Australia*
[c] *Cavendish Laboratory, University of Cambridge, J.J. Thomson Avenue, Cambridge, CB3 0HE, United Kingdom*

E-mail: B.C.Allanach@damtp.cam.ac.uk, corbett.t.s@gmail.com, dolan@unimelb.edu.au, tty20@cam.ac.uk

Abstract: We further investigate the case where new physics in the form of a massive Z' particle explains apparent measurements of lepton flavour non-universality in $B \to K^{(*)}l^+l^-$ decays. Hadron collider sensitivities for direct production of such Z's have been previously studied in the narrow width limit for a $\mu^+\mu^-$ final state. Here, we extend the analysis to sizeable decay widths and improve the sensitivity estimate for the narrow width case. We estimate the sensitivities of the high luminosity 14 TeV Large Hadron Collider (HL-LHC), a high energy 27 TeV LHC (HE-LHC), as well as a potential 100 TeV future circular collider (FCC). The HL-LHC has sensitivity to narrow Z' resonances consistent with the anomalies. In one of our simplified models the FCC could probe 23 TeV Z' particles with widths of up to 0.35 of their mass at 95% confidence level (CL). In another model, the HL-LHC and HE-LHC cover sizeable portions of parameter space, but the whole of perturbative parameter space can be covered by the FCC.

Keywords: Beyond Standard Model, GUT

ArXiv ePrint: 1810.02166

[1] Corresponding author.

https://doi.org/10.1007/JHEP03(2019)137

JHEP03(2019)137

Contents

1 Introduction

Over the past number of years, there has been much interest in a number of anomalies[1] in flavour physics. Specifically, the ratio of branching ratios (BRs)

$$R_K \equiv \frac{BR(B \to K\mu^+\mu^-)}{BR(B \to Ke^+e^-)}, \qquad R_{K^*} \equiv \frac{BR(B \to K^*\mu^+\mu^-)}{BR(B \to K^*e^+e^-)}, \tag{1.1}$$

have substantial deviations from Standard Model (SM) expectations [1, 2]. There are also discrepancies in the angular variable P_5' [3, 4] and $BR(B_s \to \phi\mu^+\mu^-)$. It is by now well known that it is possible to account for these anomalies through the existence of new physics which contributes to the neutral current $b \to s\mu^+\mu^-$ decay channel [5–12].

The most well-studied UV-complete explanations of these anomalies involve either flavour-violating Z's and/or leptoquarks. We shall focus here on the Z' scenario. Models falling into this category involve a new gauge group beyond the SM. This could be an abelian extension such as $L_\mu - L_\tau$ and related gauge groups [13–41], or the new gauge group could be non-abelian [14], leading to the existence of W' particles, for example. There are also models with multiple abelian groups [42] leading to multiple Z' particles. Most of these models involve generating the $b \to s\mu^+\mu^-$ transition at tree-level, although

[1] In the present paper, we use 'anomaly' to refer to a tension between an experimental measurement and its Standard Model prediction.

JHEP03(2019)137

a loop-level penguin is also possible [43], which requires a much lighter Z' due to the loop suppression.

While one can study the effects of these models on flavour physics indirectly using effective field theory, one would also like to pin down the properties of the new resonances through their direct production in a high energy collider environment. This raises the exciting prospect of

> *directly experimentally probing the new physics that explains aspects of the fermion mass problem* [44–46]

(i.e. the patterns and hierarchies in fermion masses and mixing parameters). It has previously been argued that perturbative unitarity requires that the new physics responsible for the flavour anomalies must enter at a scale below 80 TeV [7]. Other phenomenological bounds, notably from the measurement of $B_s - \overline{B_s}$ mixing, imply a stricter upper bound for perturbative values of the Z' coupling if one wants to simultaneously fit $R_{K^{(*)}}$. Accordingly, one may hope that the resonances may be accessible at a future hadron collider, or at the High-Luminosity Large Hadron Collider (HL-LHC).

In ref. [47], sensitivities of future hadron colliders were estimated for particles that can explain the R_K and $R_{K^{(*)}}$ measurements. In particular, ref. [47] considers the case where the anomalies are explained by a Z' or leptoquark, each with flavour dependent couplings. The $\mu^+\mu^-$ channel was used for the Z' case. Simplifications in the analysis (an extrapolation of current LHC search limits, assuming that acceptances and efficiencies don't change with centre of mass energy) required also that the decay width of a new s-channel resonance was narrow (defined to be less than 10% of its mass). However, a substantial region of the parameter space which fits the B-anomalies requires large $\mathcal{O}(1)$ couplings which lead to large decay widths. Moreover, the high-luminosity run of the LHC may yet see indirect signs of new physics from effective operators in the high invariant mass tail of di-lepton distributions [48, 49]. We shall see that such a large effect would typically imply an underlying wide resonance.

Therefore, in this paper, we study the reach and implications of the fat, flavourful Z' scenario, taking effects of the large width into account in our simulations. By simulating Z' signal events, we also take into account changes in acceptances and efficiencies when operating at different centre of mass energies. We study the phenomenology of two $\mathrm{SU}(2)_L$ invariant simplified models, which we dub the Mixed Up-Muon and Mixed Down-Muon models, leaving the study of large-width leptoquarks to future work.[2]

We focus our attention on the HL-LHC, the High-Energy LHC (HE-LHC), and the Future Circular Collider (FCC). We find that while the HL-LHC is sensitive only to narrow ($\Gamma_{Z'}/M_{Z'} < 0.1$) resonances, the HE-LHC and FCC could probe fat, flavourful resonances with widths of up to 35% of the mass for Z' masses up to 23 TeV for the Mixed-Up

[2]We note that other types of new particles have been proposed to resolve the tension between measurements and SM predictions of B to $D^{(*)}\tau\nu$ decays [50–56]. These particles (e.g. W's or other types of leptoquark) must be much lighter or much more strongly coupled than the ones responsible for the $bs\mu^+\mu^-$ anomalies in order to fit data, and so should be consequently easier to detect. The study of these other types of particles is also left to future work.

JHEP03(2019)137

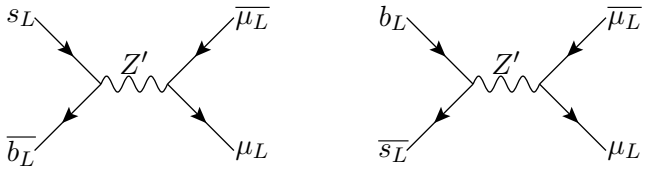

Figure 1. Feynman diagrams of parton interactions in pp collisions where a flavourful Z' produces a $\mu^+\mu^-$ final state. In the low momentum limit, the same diagrams generate an effective operator capable of accounting for the discrepancies in $B \to K^{(*)}\mu^+\mu^-$ decays as compared to SM predictions.

Muon model, and the entire perturbative region of parameter space for the Mixed-Down Muon model.

We proceed as follows: in section 2 we develop simplified Z' models for the B-anomalies and detail the other important constraints such as meson mixing, neutrino trident production, and indirect effects in the di-muon invariant mass distribution. In section 3 we present our projections on future collider sensitivity to these models before concluding in section 4. Our notation for the fields is listed in appendix A by detailing their SM quantum numbers.

2 Simplified models

We consider two representative models of Z's, following ref. [47], which introduced the naïve and the $33\mu\mu$ models. The tree-level Z' Lagrangian couplings that we know must be present in Z' models in order to explain the neutral current B-anomalies are

$$\mathcal{L}_{Z'f} = \left(g_{sb} Z'_\rho \overline{s_L}\gamma^\rho b_L + \text{h.c.}\right) + g_{\mu\mu} Z'_\rho \overline{\mu_L}\gamma^\rho \mu_L + \ldots \tag{2.1}$$

In fact, models where the Z' couples equally to left- and right-handed muons has as good a fit [11] (models where the Z' couples solely to right-handed muons are disfavoured because they predict an *enhancement* in $R_{K^{(*)}}$ rather than a diminution). Our results later, based on direct Z' production followed by subsequent decay into $\mu^+\mu^-$, do not depend upon the spin of the muon coupling, to a good approximation and so our results also cover the vector-like coupling case. A fit to $R_{K^{(*)}}$ and other 'clean[3]' B-anomalies in ref. [11] found that the couplings and masses of Z' particles are constrained to be

$$g_{bs} g_{\mu\mu} = -x \left(\frac{M_{Z'}}{31\text{TeV}}\right)^2, \tag{2.2}$$

if g_{bs} and $g_{\mu\mu}$ are real, where $x = 1.00 \pm 0.25$. Throughout this paper, we shall enforce eq. (2.2), taking the central value $x = 1.00$ from the fit. In general, g_{bs} and $g_{\mu\mu}$ are complex. However, here, we take $g_{\mu\mu}$ to be real and positive and g_{bs} to be negative. In the models we introduce below, g_{bs} may have a small imaginary part. Since the full effects of complex phases are outside the scope of this work, whenever we refer to g_{bs} below, we shall implicitly refer to its absolute value.

JHEP03(2019)137

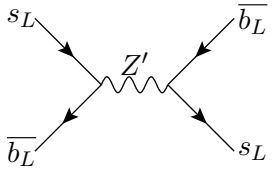

Figure 2. Feynman diagram of the tree-level Z' contribution to $B_s - \overline{B_s}$ mixing.

2.1 Constraints

Z' models are subject to a number of constraints, the strongest being from measurements of $B_s - \overline{B_s}$ mixing, which constrains a function of g_{bs} and $M_{Z'}$. A Feynman diagram depicting the Z' contribution is shown in figure 2. Another constraint comes from neutrino trident production which is sensitive to $g_{\mu\mu}$ and $M_{Z'}$. We adapt the bound on B_s-mixing from ref. [57], using the 2σ constraint derived from the 2016 FLAG average on the hadronic form factor f_{B_s} and bag parameter B_{B_s}. More recently, the Fermilab/MILC Collaboration has presented another determination [58] of these non-perturbative parameters substantially higher than previous results which means that the $B_s - \overline{B_s}$ mixing measurement would be in tension with inferred SM predictions. This would imply a much stronger bound on Z's (which would have the wrong sign contribution to explain the tension) [30, 59–61]. The result from ref. [61] is equivalent to

$$|g_{bs}| \lesssim M_{Z'}/(600 \text{ TeV}). \tag{2.3}$$

We shall display this bound and the bound from pre-2016: $|g_{bs}| \lesssim M_{Z'}/(148 \text{ TeV})$ in order to be conservative. Eqs. (2.2) and (2.3) imply

$$\frac{|g_{\mu\mu}|}{|g_{bs}|} \gtrsim 374x, \tag{2.4}$$

whereas the pre-2016 bound would imply $|g_{\mu\mu}|/|g_{bs}| \gtrsim 31x$. We also take into account neutrino trident production, $\nu_\mu \gamma^* \to \nu_\mu \mu^+ \mu^-$, using the constraints on leptonic operators in the SM effective field theory (EFT) from refs. [62, 63]. This corresponds to $g_{\mu\mu} \lesssim M_{Z'}/(0.39 \text{ TeV})$ which sets an upper bound on the muon coupling for low $m_{Z'}$. This upper bound is not strong enough to affect our projections to future colliders.

2.2 Model definition and couplings

Including only the Z' couplings in eq. (2.1) without the ellipsis was called the naïve model in ref. [47]. However, we now introduce a new similar simplified model that respects $\mathrm{SU}(2)_L$. In order to do this, we must first set up the mass eigenbasis and the weak eigenbasis. Writing the SM weak eigenbasis fermionic fields with a prime (see appendix A for the field definitions):

$$\mathbf{u'_J} = \begin{pmatrix} u'_J \\ c'_J \\ t'_J \end{pmatrix}, \qquad \mathbf{d'_J} = \begin{pmatrix} d'_J \\ s'_J \\ b'_J \end{pmatrix}, \qquad \mathbf{n'_L} = \begin{pmatrix} \nu_{e\,L}' \\ \nu_{\mu\,L}' \\ \nu_{\tau\,L}' \end{pmatrix}, \qquad \mathbf{e'_J} = \begin{pmatrix} e'_J \\ \mu'_J \\ \tau'_J \end{pmatrix},$$

[3] i.e. observables with small theoretical uncertainties in their predictions.

JHEP03(2019)137

where $J \in \{L,\ R\}$. We write the Standard Model fermionic electroweak doublets as

$$\mathbf{Q'_{L}}_i = \begin{pmatrix} \mathbf{u'_{L}}_i \\ \mathbf{d'_{L}}_i \end{pmatrix}, \qquad \mathbf{L'_{L}}_i = \begin{pmatrix} \mathbf{n'_{L}}_i \\ \mathbf{e'_{L}}_i \end{pmatrix}.$$

In order to change the naïve model to respect $\mathrm{SU}(2)_L$, we begin by defining couplings to the fermionic electroweak doublet fields

$$\mathcal{L}_{Z'f} = \left(\overline{\mathbf{Q'_{L}}_i} \lambda^{(Q)}_{ij} \gamma^\rho \mathbf{Q'_{L}}_j + \overline{\mathbf{L'_{L}}_i} \lambda^{(L)}_{ij} \gamma^\rho \mathbf{L'_{L}}_j \right) Z'_\rho, \tag{2.5}$$

where we have used the Einstein summation convention over the family indices $i, j \in \{1,\ 2,\ 3\}$ as well as over the vector index ρ but we have omitted gauge labels. $\lambda^{(Q)}$ and $\lambda^{(L)}$ are Hermitian dimensionless 3 by 3 matrices of coupling constants. Their structure will be decided by the Z' ultra-violet completion (for example they will be diagonal if it derives from an abelian group). For now we remain agnostic as to their structure, in the spirit of simplified model building. We shall later fix them to give simple couplings in the mass eigenbasis.

In order to do this, we write the terms of the Lagrangian leading to fermion masses as

$$-\mathcal{L}_Y = \overline{\mathbf{Q'_{L}}} Y_u \phi^c \mathbf{u'_{R}} + \overline{\mathbf{Q'_{L}}} Y_d \phi \mathbf{d'_{R}} + \overline{\mathbf{L'_{L}}} Y_e \phi \mathbf{e'_{R}} + \frac{1}{2} (\mathbf{L'_{L}}^{\,c} \phi) M^{-1} (\mathbf{L'_{L}} \phi) + \text{h.c.} \tag{2.6}$$

where ϕ is the SM Higgs doublet[4] and Y_u, Y_d, Y_e are 3 by 3 complex dimensionless Dirac mass matrices for the up-type quarks, the down-type quarks and the charged leptons, respectively and M^{-1} is a 3 by 3 complex symmetric matrix of mass dimension -1. The last term is a dimension 5 non-renormalisable operator that yields left-handed Majorana neutrino masses. It may result from integrating out heavy right-handed neutrinos, or lepton number violating sparticles, for example. After electroweak symmetry breaking, the terms in eq. (2.6) become the fermion mass terms plus some Higgs interactions:

$$\begin{aligned} -\mathcal{L}_Y = {} & \overline{\mathbf{u'_{L}}} V_{u_L} V_{u_L}^\dagger m_u V_{u_R} V_{u_R}^\dagger \mathbf{u'_{R}} + \overline{\mathbf{d'_{L}}} V_{d_L} V_{d_L}^\dagger m_d V_{d_R} V_{d_R}^\dagger \mathbf{d'_{R}} \\ & + \overline{\mathbf{e'_{L}}} V_{e_L} V_{e_L}^\dagger m_e V_{e_R} V_{e_R}^\dagger \mathbf{e'_{R}} + \overline{\mathbf{n'_{L}}^{\,c}} V_{\nu_L}^* V_{\nu_L}^T m_\nu V_{\nu_L} V_{\nu_L}^\dagger \mathbf{n'_{L}} + \text{h.c.} + \ldots \end{aligned} \tag{2.7}$$

where V_{X_L} and V_{X_R} are 3 by 3 unitary matrices, $\mathbf{n'_{L}}^{\,c}$ is the charge conjugate of the left-handed neutrino field, $m_u = vY_u$, $m_d = vY_d$, $m_e = vY_e$ and $m_\nu = v^2 M^{-1}$. v is the vacuum expectation value of the neutral component of ϕ.

Choosing $V_{X_L}^\dagger m_X V_{X_R}$ to be diagonal, real and positive for $X \in \{u, d, e\}$ and $V_{\nu_L}^T m_\nu V_{\nu_L}$ to be diagonal, real and positive for the neutrinos (all in increasing order of mass toward the bottom right of the matrix), we can identify the *non*-primed mass eigenstates

$$\begin{aligned} &\mathbf{u_R} \equiv V_{u_R}^\dagger \mathbf{u_R}', \qquad &&\mathbf{u_L} \equiv V_{u_L}^\dagger \mathbf{u_L}', \qquad &&\mathbf{d_R} \equiv V_{d_R}^\dagger \mathbf{d_R}', \qquad &&\mathbf{d_L} \equiv V_{d_L}^\dagger \mathbf{d_L}', \\ &\mathbf{e_R} \equiv V_{e_R}^\dagger \mathbf{e_R}', \qquad &&\mathbf{e_L} \equiv V_{e_L}^\dagger \mathbf{e_L}', \qquad &&\mathbf{n_L} \equiv V_{\nu_L}^\dagger \mathbf{n_L}'. \end{aligned}$$

We may then identify the Cabibbo-Kobayashi-Maskawa matrix V and the Pontecorvo-Maki-Nakagawa-Sakata matrix U:

$$V = V_{u_L}^\dagger V_{d_L}, \qquad U = V_{\nu_L}^\dagger V_{e_L}. \tag{2.8}$$

[4] ϕ^c denotes $(\phi^{0*},\ -\phi^{+*})^T$.

JHEP03(2019)137

Then eq. (2.5) becomes

$$\mathcal{L} = \left(\overline{\mathbf{u_L}} V \Lambda^{(Q)} V^\dagger \gamma^\rho \mathbf{u_L} + \overline{\mathbf{d_L}} \Lambda^{(Q)} \gamma^\rho \mathbf{d_L} + \overline{\mathbf{n_L}} U \Lambda^{(L)} U^\dagger \gamma^\rho \mathbf{n_L} + \overline{\mathbf{e_L}} \Lambda^{(L)} \gamma^\rho \mathbf{e_L} \right) Z'_\rho, \tag{2.9}$$

where we have defined the 3 by 3 dimensionless coupling matrices

$$\Lambda^{(Q)} \equiv V_{d_L}^\dagger \lambda^{(Q)} V_{d_L}, \qquad \Lambda^{(L)} \equiv V_{e_L}^\dagger \lambda^{(L)} V_{e_L}. \tag{2.10}$$

2.3 The 'mixed up-muon' (MUM) model

In order to obtain the couplings in eq. (2.1), we set

$$\Lambda^{(Q)} = g_{bs} \begin{pmatrix} 0 & 0 & 0 \\ 0 & 0 & 1 \\ 0 & 1 & 0 \end{pmatrix}, \qquad \Lambda^{(L)} = g_{\mu\mu} \begin{pmatrix} 0 & 0 & 0 \\ 0 & 1 & 0 \\ 0 & 0 & 0 \end{pmatrix}, \tag{2.11}$$

where in the ultra-violet completion we may expect g_{bs} and $g_{\mu\mu}$ to be related in some way, but in our simplified model we leave them free and to be determined by data. By the choice in eq. (2.11), we retain the desired Z' couplings in the down quarks and charged leptons of eq. (2.1), but these come with $\mathrm{SU}(2)_L$-respecting mixed couplings to up quarks and neutrinos. From now on, we refer to eqs. (2.9), (2.11) as the 'mixed-up muon' model. The inclusion of neutrinos into the model means that the Z' has a lower BR into muons than the naïve model: the Z' BR to muon pairs is identical to that into neutrinos, to a very good approximation.

2.4 The 'mixed down-muon' (MDM) model

Here, we simply make a different choice for $\Lambda^{(Q)}$, but the same choice as MUM for $\Lambda^{(L)}$:

$$\Lambda^{(Q)} = g_{tt} V^\dagger \cdot \begin{pmatrix} 0 & 0 & 0 \\ 0 & 0 & 0 \\ 0 & 0 & 1 \end{pmatrix} \cdot V, \qquad \Lambda^{(L)} = g_{\mu\mu} \begin{pmatrix} 0 & 0 & 0 \\ 0 & 1 & 0 \\ 0 & 0 & 0 \end{pmatrix}. \tag{2.12}$$

This is just a rewriting of the $33\mu\mu$ model in ref. [47], but we call it the 'mixed-down muon' model as it better fits with our chosen nomenclature above. The MDM model differs from the MUM model in that the Z' has various couplings to mixed down-type quarks (and to the left-handed top). It thus constitutes a different case for study. Matching $\Lambda^{(Q)}$ here with eq. (2.1) identifies

$$g_{bs} = V_{ts}^* V_{tb} g_{tt}. \tag{2.13}$$

$g_{tt} > 0$ ensures $g_{bs} < 0$ as required by eq. (2.2), since $V_{ts} \approx -0.04$ and $V_{tb} \approx 1$. Since $|V_{ts}^* V_{tb}| \approx 0.04 \ll 1$, this model helps explain why the Z' model couples more weakly to $\overline{b_L} s_L + \text{h.c.}$ as compared to $\overline{\mu_L} \mu_L$, making the $B_s - \overline{B_s}$ mixing constraint in eq. (2.3) easier to satisfy at the same time as eq. (2.2). A more complete MDM type model is provided by the Third Family Hypercharge Model example case [45], which predicts that the relevant couplings have similar structure to those in eq. (2.12) (along with other couplings to third generation fermions and mixed neutrinos and small violations of flavour universality in the Z couplings).

Both the MDM and the MUM model generate the Feynman diagrams for hadron collider di-muon production shown in figure 1 (along with additional production diagrams from other quarks).

JHEP03(2019)137

2.5 Decays

The Z' partial width for decays into massless fermions f_i and $\overline{f_j}$ is given by

$$\Gamma_{f_i f_j} = \frac{C}{24\pi} |g_{f_i f_j}|^2 M_{Z'} \,, \tag{2.14}$$

where the constant $C = 3$ for coloured fermions and $C = 1$ for colour singlet fermions. In the models we study (defined by the couplings in eqs. (2.11), (2.12) and eq. (2.9)) we sum over decays to all of the SM fermions that the Z' couples to. Given the requirements on the couplings to fit the flavour anomalies, the decay width is dominated by decays to muons and neutrinos for both the MUM and the MDM models. In the limit that the fermion masses are small compared to $M_{Z'}$ (this will be a good approximation in the domain of parameter space we consider), eq. (2.14) implies that the BRs are independent of $M_{Z'}$.

We show in figure 3 the width Γ as a function of $M_{Z'}$ and $g_{\mu\mu}$ for the MUM (left panel) and MDM (right panel) models, with the region in red ruled out by the constraint from B_s-mixing. This forces $|g_{bs}|$ to be small, except when $M_{Z'}$ is large. We also note that the relative width increases rapidly with $M_{Z'}$ in the MDM model. This is because in the MDM model, as $M_{Z'}$ becomes large, g_{tt} is driven to be large by eqs. (2.13) and (2.2). Because the $\bar{b}s$ coupling is unsuppressed by a CKM mixing element in the MUM model, we do not see the effect there. In our simplified models, it could also be sensible to add additional couplings of the Z' (these are often present in specific models). In that case, one could consider the width to be a free parameter with a minimum value given by the simplified model value shown in figure 3. A larger relative width, if it is larger than the experimental resolution, typically means that the sensitivity is reduced and searches are consequently more challenging.

In the MUM model, eq. (2.4) means that the Z' decays with a 50% BR to muon pairs and a 50% BR to neutrinos, to a good approximation. However, in the MDM model, $|g_{tt}| = |g_{bs}|/|V_{ts}^* V_{tb}|$ enhances the coupling to quarks: putting in the central values $|V_{ts}| = 0.04$, $|V_{tb}| = 1$ for the magnitudes of CKM matrix elements yields $y \equiv |g_{tt}|/|g_{\mu\mu}| < 0.6$. The BR into quarks in the MDM model is then approximately

$$z \equiv \sum_{i,j=1}^{3} BR(Z' \to q_i \bar{q}_j) = \frac{3y^2}{1+y^2}, \tag{2.15}$$

which can be as high as 52%. The remainder of the decays are again split equally between muon pairs and neutrino pairs. We summarise the BRs for both the MUM model and the MDM model in table 1. Since it is difficult or impossible to discriminate the flavour of light jets, we have lumped them all together. The table already suggests channels to search for the Z'. Muon anti-muon pairs have a sizeable BR in any event, and will be the primary search channel, being the most closely related channel to the explanation of the neutral current B-anomalies. It is this channel that we shall focus on in the present paper. However, in the MDM model, a sizeable BR to boosted top anti-top pairs is also possible, and the resulting boosted top pairs are an interesting channel for future study.

JHEP03(2019)137

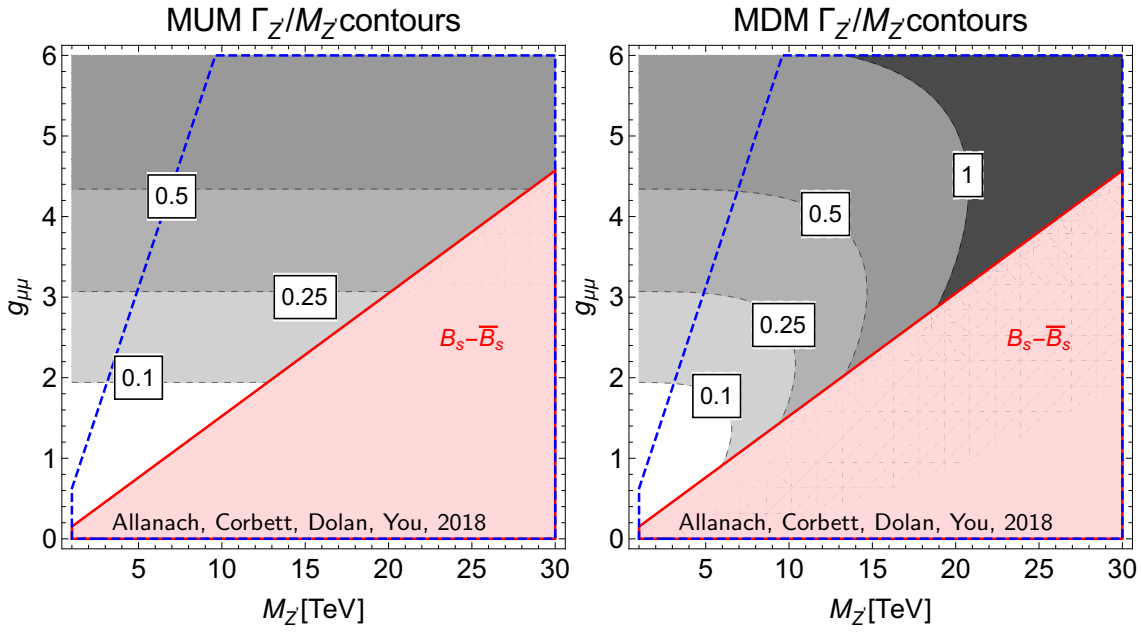

Figure 3. Width of the Z' as a fraction of its mass as a function of $M_{Z'}$ and $g_{\mu\mu}$ in the MUM (left hand panel) and MDM (right hand panel) models, derived from Each point in the plane fits the neutral current B-anomalies, since eq. (2.2) with $x = 1.00$ has been enforced meaning that $g_{bs} \propto M^2_{Z'}/g_{\mu\mu}$. The black region at the top right hand panel has width greater or equal to the mass, meaning that the model has entered the non-perturbative régime, and our results (based on perturbation theory) may be inaccurate there. In order to show more of the parameter space, we have displayed the *pre-2016* B_s mixing constraint in pink and the one based on eq. (2.3), where the region below the blue dashed line is ruled out.

MUM model		MDM model							
mode	BR	mode	BR	mode	BR	mode	BR	mode	BR
$\nu_i\bar{\nu}_k$	0.5	$\nu_i\bar{\nu}_k$	$(1-z)/2$	$t\bar{t}$	$z/2$	jj'	$y^2zX/2$	bj	$y^2zY/2$
$\mu^+\mu^-$	0.5	$\mu^+\mu^-$	$(1-z)/2$	$\bar{b}b$	$y^2z\lvert V_{tb}\rvert^4/2$	$\bar{b}j$	$y^2zY/2$		

Table 1. Summary of BRs (BRs) of Z' for the MUM and MDM models. We have categorised the three lighter quarks and anti-quarks into a generic 'light' jet $j, j' \in \{u, d, s, \bar{u}, \bar{d}, \bar{s}\}$. i and $k \in \{1, 2, 3\}$ are family indices, $X \equiv \left||V_{td}|^2 + |V_{ts}|^2 + 2\Re(V^*_{ts}V_{td})\right|^2$, $Y = |V_{tb}|^2|V_{td} + V_{ts}|^2$, $y = |g_{tt}|/|g_{\mu\mu}|$ and z is defined in eq. (2.15).

2.6 Indirect sensitivity in high invariant mass di-muon tails

The Z' may be too heavy to be directly produced on-shell at the LHC. Nevertheless, it could still leave an indirect imprint in the high invariant mass di-muon tail at the LHC [48, 49]. In this case we may use an EFT approach in which we need only consider the four-fermion operators induced by integrating out the Z'. This can give an additional signal contribution to the di-muon final state above the usual SM Drell-Yan background.

We use the ATLAS data at 13 TeV with 36.1 fb^{-1} with the observed and SM number of events per bin given by table 9 of ref. [64]. Following ref. [48], we parameterise the expected

JHEP03(2019)137

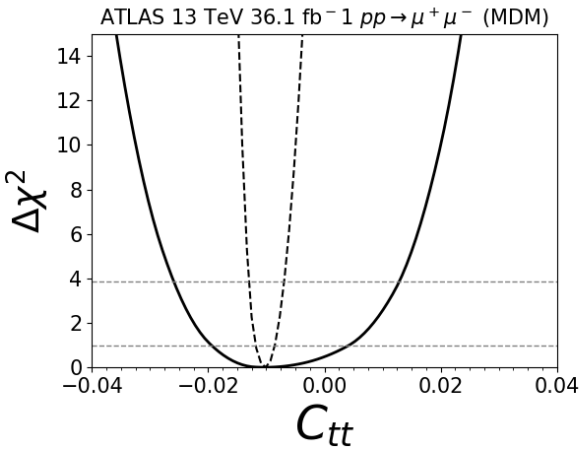

Figure 4. $\Delta\chi^2$ for the four-fermion coefficient $C_{tt} \simeq C_{bb} = -g_{bb}g_{\mu\mu}v^2/M_{Z'}^2$ from a fit to the ATLAS 13 TeV 36.1 fb^{-1} di-muon distribution in the MDM model. The high-luminosity LHC projections are shown in dashed lines.

number of events per bin as a function of the four-fermion operator coefficients $C_{q\bar{q}}$ by

$$\frac{N_{\rm bin}}{N_{\rm bin}^{\rm SM}} = \frac{\sum_{q,\bar{q}} \int_{\tau_{\rm min}}^{\tau_{\rm max}} d\tau \tau L_{q\bar{q}}(\tau,\mu_F)|F_{q\bar{q}}(\tau s, C_{q\bar{q}})|^2}{\sum_{q_i,\bar{q}_j} \int_{\tau_{\rm min}}^{\tau_{\rm max}} d\tau \tau L_{q\bar{q}}(\tau,\mu_F)|F_{q\bar{q}}^{\rm SM}(\tau s)|^2}. \tag{2.16}$$

Thus the new physics effects are only taken into account via the EFT approximation, or the signal is not sensitive to the shape of the Z' propagator. This is an approximation which is only valid when $\hat{s} \ll M_{Z'}^2$, and we must take care to delineate the domain of its validity. The sum is over all five parton flavours $q \in \{u, c, d, s, b\}$ and the parton luminosity function can be written as

$$L_{q\bar{q}}(\tau,\mu_F) = \int_\tau^1 \frac{dx}{x} f_q(x,\mu_F) f_{\bar{q}}(\tau/x,\mu_F)\,, \tag{2.17}$$

where f is the parton distribution function and μ_F the factorisation scale that we set to $\hat{s}$; we also defined $\tau \equiv \hat{s}/s$ with s the proton-proton squared centre of mass energy and $\hat{s} \equiv M_{\mu\mu}^2$. The propagator function F is given by the expression

$$F_{ij}(p^2, C_{ij}) = \delta^{ij}\left(\frac{e^2 Q_q Q_l}{p^2} + \frac{g_Z^q g_Z^l}{p^2 - M_Z^2 + iM_Z\Gamma_Z}\right) + \frac{C_{ij}}{v^2}. \tag{2.18}$$

Q_f is the electric charge of the fermion, and $g_Z^f \equiv \frac{2M_Z}{v}\left(T_f^3 - Q_f \sin^2\theta_W\right)$ where f label the species of fermion, θ_w is the SM Weinberg angle and T_f^3 is the diagonal generator of SU(2).

There was no region of 95% CL sensitivity of this high di-muon invariant mass tail analysis to the MUM model, whose signal cross-section is too small at $\sqrt{s} = 13\,\text{TeV}$, so we here focus on the sensitivity of the MDM model. Treating each bin as independently Poisson-distributed, we perform a χ^2 fit for the MDM model in which the coupling to $b\bar{b}$ is allowed to vary freely with the muon coupling fixed to $g_{\mu\mu} = 1.5$. The couplings to the other flavours are dependent on $g_{bb} \equiv g_{tt}/|V_{tb}|^2 \approx g_{tt}$ through CKM rotations, à la eq. (2.12).

JHEP03(2019)137

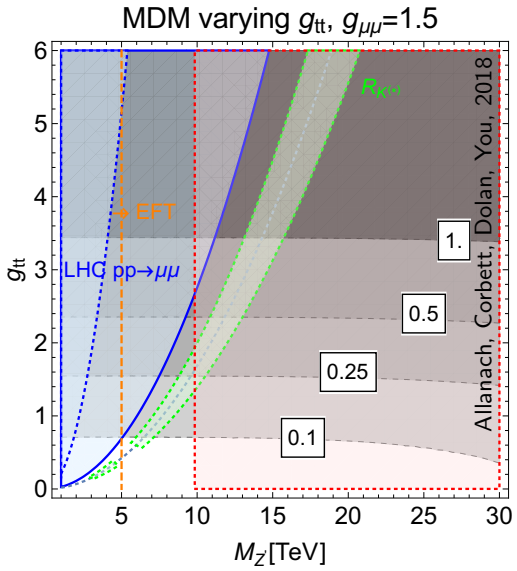

Figure 5. 95% CL exclusion region of the ATLAS 13 TeV $pp \to \mu\mu$ di-muon distribution (blue region) for 36.1 fb^{-1} (3 ab^{-1}) denoted by dotted (solid) blue lines, as a function of $M_{Z'}$ vs $g_{tt} \approx g_{bb}$ for a deformed MDM model with $g_{\mu\mu} = 1.5$. g_{bs} is fixed to its anomaly compatible value. The region of EFT validity for this analysis lies to the right of the vertical orange dotted line. Contours of $\Gamma_{Z'}/M_{Z'}$ are represented by dashed grey lines. The anomaly-compatible region within 1σ is shown in green, while the $B_s - \overline{B_S}$ mixing constraint is in red.

The resulting $\Delta\chi^2$ for the four-fermion operator coefficient $C_{tt} \simeq C_{bb} = -g_{bb}g_{\mu\mu}v^2/M_{Z'}^2$ is shown in figure 4.[5]

In figure 5, the 95% CL exclusion region of the di-muon mass distribution to a deformed MDM model is plotted as the blue region on the parameter space of $M_{Z'}$ vs g_{bb} bounded by the dotted blue curve. The deformation we consider is the removal of the connection between g_{bs} and g_{tt} in eq. (2.13): they are now considered to be independent. The dashed (solid) blue curve shows expected sensitivity for the (HL-)LHC. The vertical dashed orange line represents (approximately) where the Z' mass is beyond the direct reach of the LHC such that the EFT approach is valid. The horizontal dashed grey lines labelled by white boxes represent the width as a fraction of the Z' mass. Thus, we deduce that the blue region to the right hand side of the EFT line is ruled out by ATLAS. Should a sizeable deviation appear in the di-muon tail at the LHC (but should no resonance appear), this will be somewhere to the right-hand side of the current (dashed blue) exclusion region on the plot. In the MDM model, this along with EFT validity necessarily points towards a wide Z' ($\Gamma/M_{Z'} \geq 0.1$) to be searched for at future higher-energy colliders. Note that this conclusion is more general than the specific case of an anomaly-compatible Z', whose parameter space would then have to lie within the green band. The discovery of indirect effects that may still show up at the high-luminosity LHC therefore would provide additional motivation for studying future sensitivities to large width resonances.

[5]Switching on one operator coefficient at a time, we find limits in good agreement with those in ref. [48].

JHEP03(2019)137

3 Direct Z' sensitivity of hadron colliders

We shall here focus on the $\mu^+\mu^-$ channel for identifying fat flavourful Z' production. The $\mu^+\mu^-$ channel has the benefit of being directly involved with the inferred new physics contribution in $R_{K^{(*)}}$, and we know that its coupling $g_{\mu\mu}$ to the Z' must be much larger than $|g_{bs}|$ because of eq. (2.4). In particular models, it could be that other channels may be even more sensitive (for example to boosted top pairs), but we still restrict ourselves to the $\mu^+\mu^-$ channel because of its omnipresence in models which explain the $R_{K^{(*)}}$ measurements.

3.1 Methodology

Aside from resonance searches in the narrow width approximation [47], some previous work on the collider prospects for Z's which explain the flavour anomalies has focused on precision measurements of the high invariant mass tails of di-lepton distributions at the LHC [48, 49]. Other studies have focused on production of the resonance in association with a b-jet, exploiting the flavour structure of the Z' couplings [65, 66]. Our strategy is instead a direct search for the fat Z' resonance in the di-lepton invariant mass distribution, taking width effects correctly into account. We use the 5-flavour `NNPDF2.3LO` [67] ($\alpha_s(M_Z) = 0.119$) parton distribution functions via `LHAPDF6` [68] in order to re-sum the logarithms associated with the initial state b-quark [69]. The hadronisation scale is fixed to be $M_{Z'}$.

The standard propagator used in resonance production has the Breit-Wigner form

$$\mathcal{D}_{\mu\nu}(p^2) = \frac{-i\eta_{\mu\nu}}{p^2 - M_{Z'}^2 + i\Gamma_{Z'}M_{Z'}}, \tag{3.1}$$

where $\eta_{\mu\nu}$ is the Minkowski metric. This results from re-summing a class of corrections to the tree-level propagator. These are related to the decay width by the optical theorem. Usually, these corrections are evaluated at a fixed scale $\hat{s} = M_{Z'}^2$, in which case the propagator has the form above. However, for wide resonances the partonic centre-of-mass energy can be sufficiently far from the pole in the propagator that this approximation is no longer valid. A clear exposition of this can be found in the literature on the line-shape of the Z^0-boson [70]. In this case we must include the momentum dependence, and not just evaluate the imaginary terms at the fixed scale $\hat{s} = M_{Z'}^2$. In practical terms, this amounts to replacing $\Gamma_{Z'}M_{Z'}$ with $\frac{\hat{s}}{M_{Z'}^2}\Gamma_{Z'}M_{Z'}$, so that the corrected propagator has the form

$$\mathcal{D}_{\mu\nu}(p^2) = \frac{-i\eta_{\mu\nu}}{p^2 - M_{Z'}^2 + i\frac{p^2}{M_{Z'}^2}\Gamma_{Z'}M_{Z'}}. \tag{3.2}$$

In practice we do this by changing the Z' propagator in the `UFO` files [71] we generate[6] from `FeynRules` [72, 73]. We generate events using `MadGraph5` [74]. We show the effects of this change from the Breit-Wigner form in figure 6, which shows the di-muon invariant mass distribution for $m_{Z'} = 13, 17\,\text{TeV}$ for the Breit-Wigner and corrected propagators. We observe a smearing due to the large width effect, which reduces sensitivity somewhat.

[6] The `UFO` files are included in the ancillary information submitted with the `arXiv` version of this paper.

JHEP03(2019)137

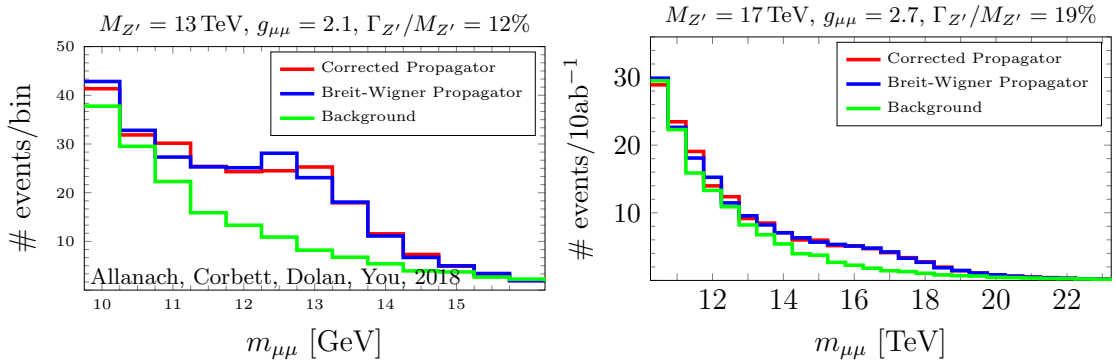

Figure 6. Expected di-muon invariant mass distributions at the FCC for (left) $M_{Z'}$=13 TeV, $g_{\mu\mu} = 2.1$ and (right) $M_{Z'}$=17 TeV, $g_{\mu\mu} = 2.7$, corresponding to widths of 12% and 19% respectively. The expected number of events per bin on the ordinate is for 10 ab^{-1} of integrated luminosity. This figure shows the difference between using the `MadGraph5` default propagator and the new propagator $\sim 1/(p^2 - M^2 - ip^2\Gamma/M)$. The significance for $M_{z'} = 13$ TeV is 8.5 (9.7 for the default propagator) summing from bin 4 (5). The significance for $M_{Z'} = 17$ TeV is 4.6 (5.6) summing from bin 9 (10). All histograms and significance calculations are post-detector simulation (i.e. `DELPHES 3`).

We define signal sensitivity as follows: first, we define a window of di-muon invariant mass in which to generate events, depending upon the collider:

$$\begin{aligned} m_{\mu\mu}^{\text{HL-LHC}} &\in [\max\{M_{Z'} - \Gamma - 500\text{ GeV},\ 100\text{ GeV}\},\ \min\{M_{Z'} + \Gamma,\ 5.9\text{ TeV}\}] \\ m_{\mu\mu}^{\text{HE-LHC}} &\in [\max\{M_{Z'} - \Gamma - 2\text{ TeV},\ 250\text{ GeV}\},\ \min\{M_{Z'} + \Gamma,\ 11.25\text{ TeV}\}] \\ m_{\mu\mu}^{\text{FCC}} &\in [\max\{M_{Z'} - \Gamma - 2\text{ TeV},\ 250\text{ GeV}\},\ \min\{M_{Z'} + \Gamma,\ 25.25\text{ TeV}\}]. \end{aligned}$$

We define $S_i \equiv (\sigma_i^{Z'+SM} - \sigma_i^{SM})\mathcal{L}$, where $\mathcal{L}$ is assumed integrated luminosity and $i \in \{1, \ldots, N\}$, as the expected number of signal events in a single bin of width W in $m_{\mu\mu}$ estimated in our simulations.[7] $W = 500$ GeV is taken for all simulations apart from the HL-LHC ones, where $W = 100$ GeV is taken. $\sigma_i^{Z'+SM}$ is the $pp \to \mu^+\mu^-$ cross-section including the Z' lying in the $m_{\mu\mu}$ bin i and σ_i^{SM} is the SM $\mu^+\mu^-$ cross-section in the same bin.[8] Each of these cross-sections is to be understood as being for $pp \to \mu^+\mu^-$ after acceptance, efficiency and detector effects. The total significance, measured in terms of 'number of σ', is defined to be

$$S = \max_i D_i, \qquad \text{where} \qquad D_i \equiv \frac{\sum_{j=i}^{N} S_j}{\sqrt{\sum_{k=i}^{N} B_k}}, \tag{3.3}$$

and the number of background events in bin k $B_k \equiv \sigma_k^{SM}\mathcal{L}$ is likely to be estimated in practice by experiments measuring control regions. However, there will be systematic errors and correlations involved with the extraction of the B_k which we do not take into account

[7] Each bin is centred on $m_{\mu\mu} = W(2n+1)/2$ GeV, where $n \in \{0, 1, 2, \ldots\}$.

[8] Although interference effects between signal and background are automatically taken into account by `MadGraph5`, in both the MUM model and the MDM model, they are CKM suppressed or parton density function-suppressed compared to the pure signal contribution.

JHEP03(2019)137

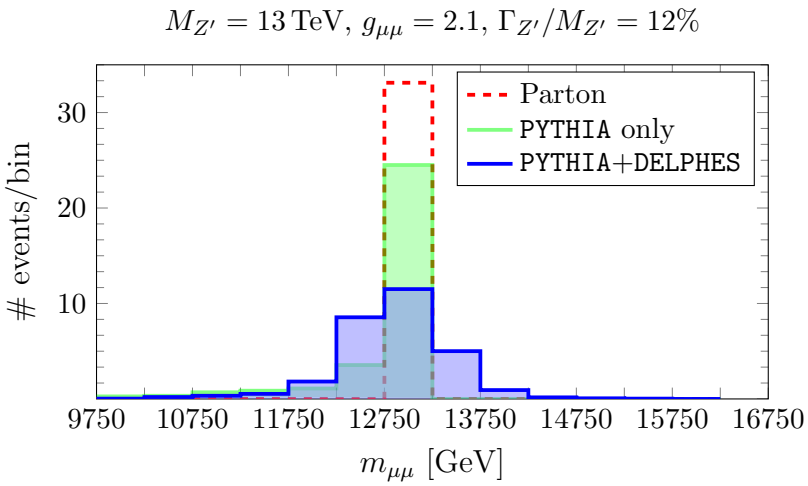

Figure 7. The bleeding of a single parton level bin centred on $m_{\mu\mu} = 13$ TeV for the Z' signal at the FCC. At parton-level, we expect 33.1 events (in 10 ab^{-1}), after parton showering effects are simulated by PYTHIA this reduces to 31.3 and after simulating detector effects with DELPHES 3, 29.2.

here. Our definition of signal significance is rather crude, and in the end if many signal events are collected, shapes and other features of signal events are likely to be used which will increase the significance. We also ignore the effects of theoretical uncertainties (parton density function errors, higher order contributions etc), which will tend to decrease the sensitivity. Despite these short-comings, at this stage our crude definition of significance will suffice for a reasonable but approximate estimate.

In order to further examine the simulated effects of parton showering and the detector, we simulate signal-only FCC collisions for $M_{Z'} = 13\,\text{TeV}$. We initially filter out all events other than those where the parton-level simulation gives di-muons in a single bin centred around $m_{\mu\mu} = 13\,\text{TeV}$, as shown in figure 7: thus we throw away the large width effects in this one plot for illustrative purposes (but we include them elsewhere in this paper). These central-bin events are then passed through PYTHIA8.2 [75, 76] in order to simulate initial state radiation and parton showering effects. We see that the initial parton-level simulation gets smeared to lower invariant masses. However, at such high $m_{\mu\mu}$, the muon resolution becomes significantly worse. This is because muon momentum is measured by the amount of bending in the magnetic field of the detector, but very high momentum muons will have small bending compared to lower energy ones. Thus, simulating such detector effects is essential in order to account for this. Here, we use the DELPHES 3 [77] fast detector simulator. We see that the detector smears $m_{\mu\mu}$ both to higher and lower values. Thus: the overall effect of initial state radiation and detector effects is smearing to higher and to lower values, with a small bias toward smaller invariant masses. Notably, this detector-level smearing was not accounted for in ref. [47], which gave a cruder estimate in the approximation that detector effects are the same in the LHC and FCC environments. Such an approximation becomes worse for larger $M_{Z'}$. For this 13 TeV bin, some 10% of signal events are lost due to acceptance and efficiencies.

JHEP03(2019)137

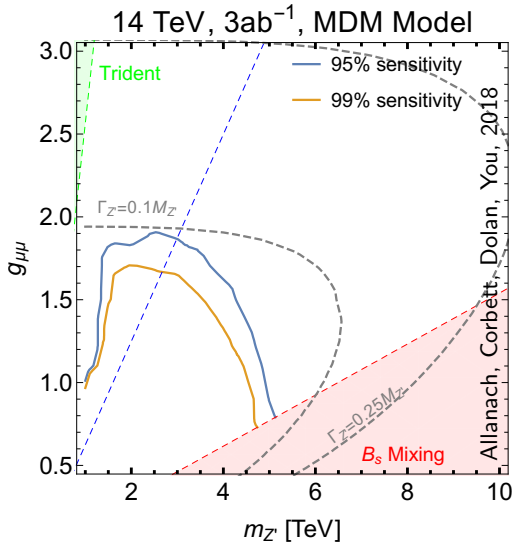

Figure 8. Predicted sensitivity for the MDM model with the 14 TeV LHC with 3/ab integrated luminosity in the $M_{Z'}$–$g_{\mu\mu}$ plane. Each point in the plane fits the neutral current B-anomalies, since eq. (2.2) with $x = 1.00$ has been enforced meaning that $g_{bs} \propto M_{Z'}^2/g_{\mu\mu}$. The solid lines show the regions of 95% CL and 99% CL sensitivity being *below* each contour. We show only the MDM model, since the HL-LHC does not have sensitivity to the allowed MUM parameter space. In order to show more of the parameter space, we have displayed the *pre-2016* B_s mixing constraint in pink and the one based on eq. (2.3), where the region below the blue dashed line is ruled out. The grey dashed lines show the values of the relative decay width $\Gamma_{Z'}/M_{Z'}$.

3.2 Results

Achieving adequate Monte-Carlo statistics in the tails of wide resonances can be challenging. We generate events in fixed-width bins of the di-muon invariant mass, so that we have good resolution in the tails. We find that generating with bin widths $W = 100, 500$ GeV as described in section 3.1 is sufficient to achieve smoothly falling distributions across the relevant range of parameter space.

The dominant background process is Drell-Yan (DY) production of di-muon pairs via γ^* and Z. While there are also contributions from di-boson production, top quarks, and vector-boson plus jets, at large invariant masses these are completely dominated by the Drell-Yan component, which makes up over 90% of the background events at the LHC [64, 78]. Accordingly, we consider DY as the only background in our simulations.

The ATLAS di-lepton search [64] sets limits on generic Z's with relative decay widths of up to 32%, by using a mass window of twice the resonance width. However, the corresponding CMS search [78] only considers narrow resonances, whose widths are up to 10% of their mass. The CMS di-jet search [79] provides limits on resonances up to 30% width, while the ATLAS di-jet searches [80] stay within the narrow regime.

We find that the 14 TeV HL-LHC with 3ab^{-1} of luminosity does not have sensitivity to the MUM model. This is due to the fact that it has small couplings, and requires a b-quark in the initial state. On the other hand, in the MDM model the Z' couples to other flavours of quark, so that the production cross-sections are substantially larger. In particular, we

JHEP03(2019)137

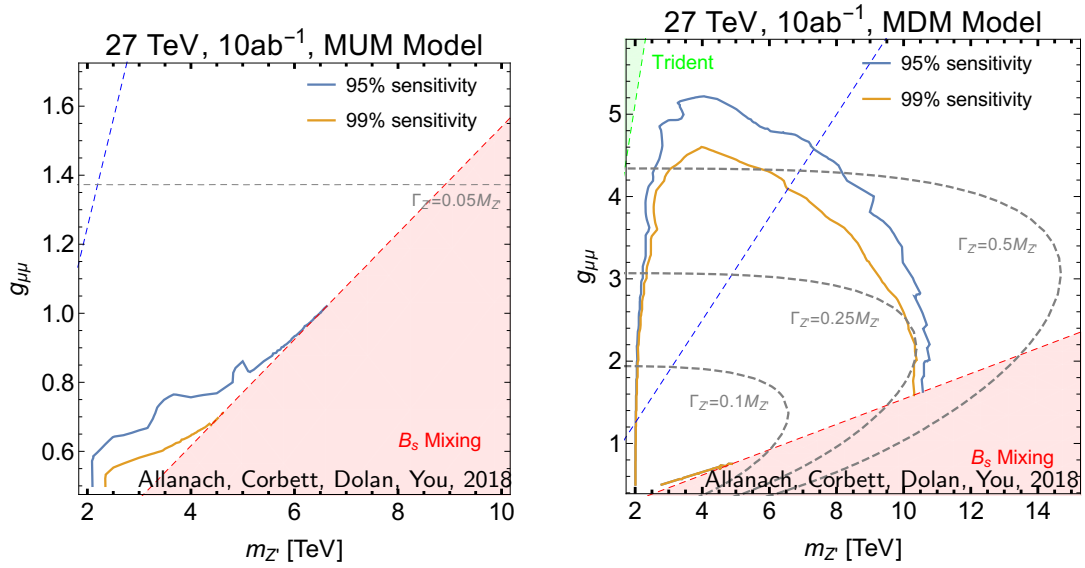

Figure 9. Predicted sensitivity for the 27 TeV HE-LHC with 15/ab integrated luminosity in the $M_{Z'}$–$g_{\mu\mu}$ plane. Each point in the plane fits the neutral current B-anomalies, since eq. (2.2) with $x = 1.00$ has been enforced meaning that $g_{bs} \propto M_{Z'}^2/g_{\mu\mu}$. The solid lines show the regions of 95% CL and 99% CL sensitivity, which are *below* each contour. The left-hand plot shows the MUM model, the right-hand plot the MDM model. In order to show more of the parameter space, we have displayed the *pre-2016* B_s mixing constraint in pink and the one based on eq. (2.3), where the region below the blue dashed line is ruled out. The grey dashed lines show contours of the relative decay width $\Gamma_{Z'}/M_{Z'}$.

find that the larger cross-sections for the MDM model are driven by $bb \to Z' \to \mu^+\mu^-$ due to the enhanced g_{bb} coupling. We show the reach for the MDM model in figure 8. The solid lines show the regions of 2σ and 3σ exclusion. The region ruled out by neutrino trident production is shown in green, and in red the region ruled out by the B_s mixing constraint [57]. While the LHC would have sensitivity in this region, we have not set limits there since it is already ruled out. The more recent determination [61] is shown as the blue-dashed line. Finally, the grey dashed lines show contours of the relative decay width $\Gamma_{Z'}/M_{Z'}$. The reach extends out to 5 TeV, and couplings $g_{\mu\mu} \approx 2$, corresponding to a width of 10%. These results are broadly in agreement with the previous projections in [47], but not as optimistic due to our taking width and detector effects into account.

The 27 TeV HE-LHC proposal has sensitivity to the MDM model, as shown in figure 9. The HE-LHC could probe masses of up to 12 TeV and widths of up to 60% in the MDM model. However, in the MUM model, the HE-LHC has no sensitivity to the region above the blue line that is consistent with the latest B_s mixing bound. In the case that this bound becomes less stringent with more CKM and lattice data, masses up to 6 TeV for the MUM model may be covered. The exclusion contours in the figure 9 have quite different shapes, which stems from the different mixings and couplings in each model, the requirement that the couplings can explain the flavour anomalies and the different widths over the parameter spaces (as in figure 3). The lack of sensitivity at low masses is due to larger backgrounds that reduce the sensitivity to large widths.

JHEP03(2019)137

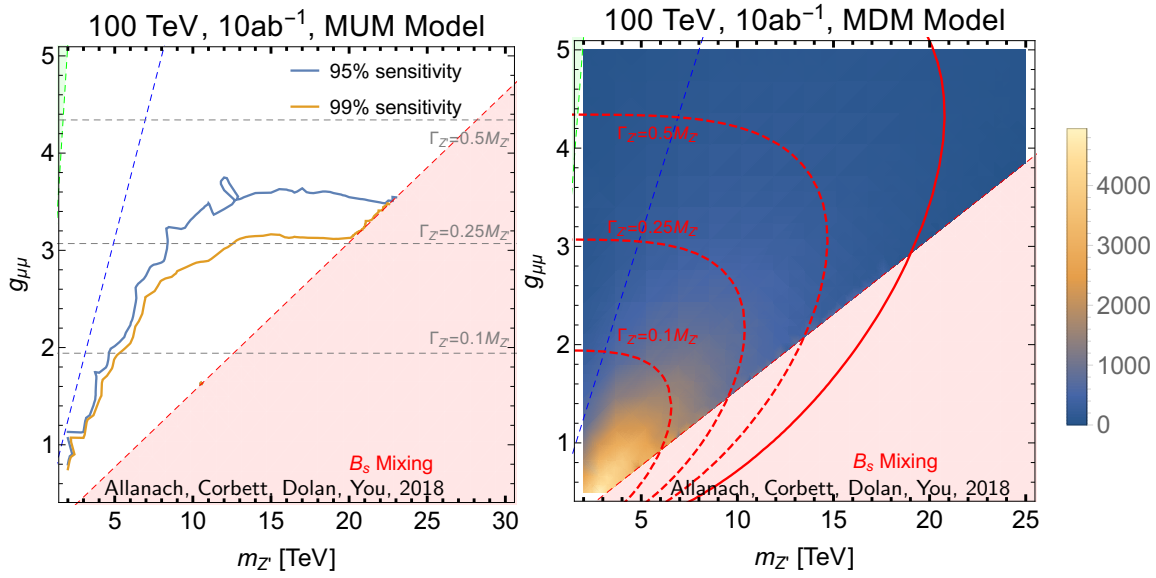

Figure 10. Predicted sensitivity for the 100 TeV FCC with 10/ab integrated luminosity in the $M_{Z'}$–$g_{\mu\mu}$ plane for the MUM model (left). Each point in the plane fits the neutral current B-anomalies, since eq. (2.2) with $x = 1.00$ has been enforced meaning that $g_{bs} \propto M_{Z'}^2/g_{\mu\mu}$. The solid lines in the left-hand panel show the regions of 95% CL and 99% CL sensitivity being *below* each contour. In order to show more of the parameter space, we have displayed the *pre-2016* B_s mixing constraint in pink and the one based on eq. (2.3), where the region below the blue dashed line is ruled out. The grey dashed lines show contours of the relative decay width $\Gamma_{Z'}/M_{Z'}$. The MDM model's significance S is colour-coded with the legend on the right; its sensitivity is $S > 10\sigma$ everywhere on the plane (right).

Finally, figure 10 shows the predicted sensitivity in the $M_{Z'}$–$g_{\mu\mu}$ plane for the FCC with 10ab^{-1} integrated luminosity. We show the MUM model on the left in the range $M_{Z'} \leq 30\,\text{TeV}$ and $g_{\mu\mu} \leq 5\,\text{TeV}$. We note that in the case where we take the latest lattice results on non-perturbative parameters (i.e. eq. (2.3)), the MUM has no sensitivity. If this bound relaxes in the future, we note that the FCC has sensitivity to the MUM model in parameter space not currently ruled out for $M_{Z'}$ up to 23 TeV and for widths up to 35%, corresponding to $g_{\mu\mu} \sim 3.5$. *All* of the MDM parameter plane in the right-handed panel of figure 3 is above 10σ significance. However, for the region of large $M_{Z'} \gtrsim 18\,\text{TeV}$ *and* $g_{\mu\mu} \gtrsim 3$, $\Gamma_{Z'} \geq M_{Z'}$ and so perturbation theory is no longer valid.

4 Conclusion

The $R_{K^{(*)}}$ flavour anomalies (discrepancies between SM predictions and experimental measurements in certain B-meson decays) are of considerable current interest and, at face value, require the existence of physics beyond the SM. One possibility involves the existence of a Z', a new heavy vector-boson with flavour dependent couplings. If the anomalies are confirmed it would be desirable to directly produce and identify whatever new particles are responsible at a current or future collider. In this work we have estimated the sensitiv-

JHEP03(2019)137

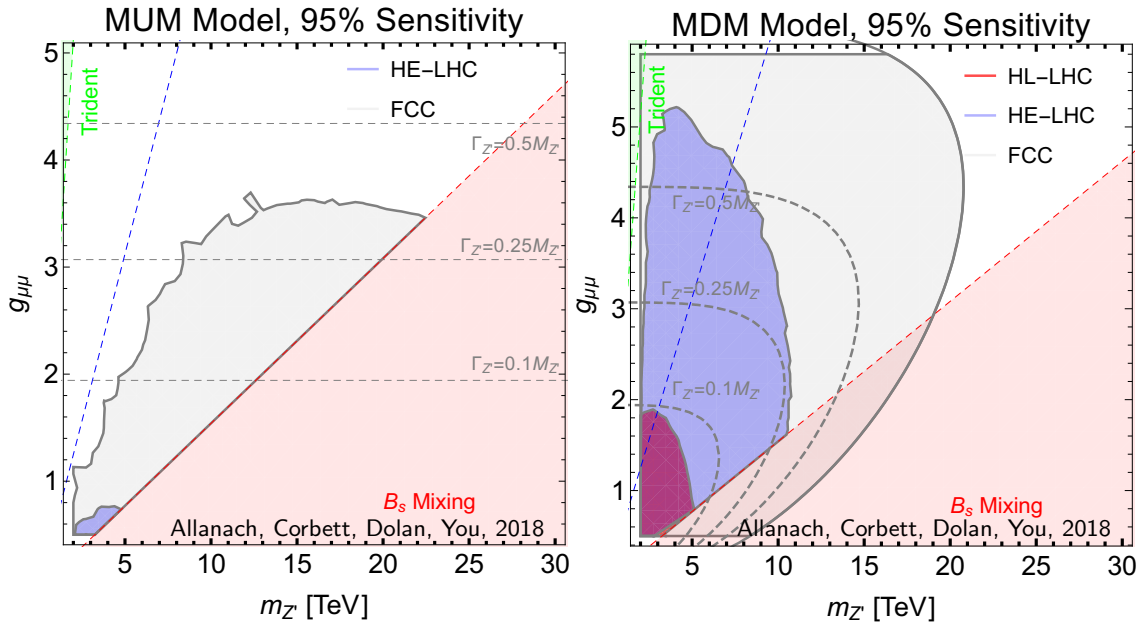

Figure 11. Summary of MUM model and MDM model 95% sensitivities for future hadron colliders: the 100 TeV FCC with 10/ab integrated luminosity, 27 TeV HE-LHC with 15/ab and the 14 TeV LHC with 3/ab integrated luminosity. Each point in the plane fits the neutral current B-anomalies, since eq. (2.2) with $x = 1.00$ has been enforced meaning that $g_{bs} \propto M_{Z'}^2/g_{\mu\mu}$. The solid lines show the regions of 95% CL and 99% CL sensitivity being *below* each contour. The region ruled out by the B_s mixing constraint [57] is shown in red while the region derived from ref. [61] would be below the blue-dashed line. The grey dashed lines show the values of the relative decay width $\Gamma_{Z'}/M_{Z'}$. The FCC reach is shown in grey and extends throughout the whole perturbative region where $\Gamma_{Z'}/M_{Z'} < 1$ in the MDM model.

ities of the HL-LHC, HE-LHC and FCC proposals to new, flavour-violating Z's capable of explaining the flavour anomalies.

The neutral current B-anomalies may require large Z' couplings depending on $M_{Z'}$, and hence involve resonances with large decay widths: fat, flavourful Z's. These widths are larger than what is usually considered in current LHC searches.

We have developed $\mathrm{SU}(2)_L$ respecting simplified models which include the couplings necessary to explain R_K and $R_{K^{(*)}}$ (and related) measurements. We pursued two models: the MUM and MDM scenarios. These differ in whether CKM mixing occurs in the up-quark or the down-quark sector. Our projections improve upon previous work [47] by including a dynamical width for the resonance and by modelling detector acceptance and efficiency effects. Although we have presented our results strictly in terms of the MUM and MDM models, any future dedicated studies should bear in mind that the width could be larger than predicted in the model in question by the Z' having more couplings than just those in eq. (2.9). Therefore, the width could be kept as an additional free parameter in any such studies. Generally, the MDM model has far more sensitivity than the MUM model. Although the additional valence quark couplings are CKM suppressed in the MDM model as compared to g_{bs}, the coupling to $b\bar{b}$ is CKM *enhanced*: a factor $1/|V_{ts}| \approx 25$ larger

JHEP03(2019)137

than g_{bs}. Z' production is then dominantly via $b\bar{b} \to Z'$, so it would be important to pin down the b-quark parton distribution functions as well as possible in order to reduce the theoretical uncertainty in the production cross-section.

Our main results are combined in figure 11, which shows the projected reach of our chosen colliders in the $M_{Z'}$–$g_{\mu\mu}$ plane. In order to achieve 95% CL sensitivity requires going beyond the HL-LHC to a higher energy machine for the MUM model. Higher energy colliders also have substantially increased mass reach for these resonances: up to 23 TeV for a resonance with 35% width in the MUM scenario. We note the importance of the accurate estimation of important non-perturbative parameters used as inputs to $B_s - \overline{B_s}$ constraints: the *pre-2016* bound is shown by the pink triangular region to the lower right hand side of the plot, but one recent determination would move the bound instead to be below the blue dashed line, removing all viable parameter space where one has 95% sensitivity to the MUM model, for instance.

We await confirmation [81] of $R_{K^{(*)}}$ flavour anomalies by analyses of LHCb Run II data and an independent check from Belle II [82]. In the event of such a confirmation, our work makes the conclusion of ref. [47] more robust, and extends it to the large width Z' case: the neutral current flavour anomalies and sensitivity to Z' particles provide another good motivation to the already strong case for future high-energy hadron colliders.

Acknowledgments

We thank other members of the Cambridge SUSY Working Group and A Greljo for helpful advice and comments and M Mangano for suggesting the project. This work has been partially supported by STFC consolidated grant ST/P000681/1. TY is supported by a Branco Weiss Society in Science Fellowship and a Research Fellowship from Gonville and Caius College, Cambridge. TC and MJD are supported by the Australian Research Council.

A Field definitions

We use the following field definitions in terms of representations of $\mathrm{SU}(3) \times \mathrm{SU}(2)_L \times \mathrm{U}(1)_Y$:

$$\begin{aligned} \mathbf{Q'_L} &= (3,\ 2,\ +1/6), & \mathbf{L'_L} &= (1,\ 2,\ -1/2), & \mathbf{e'_R} &= (1,\ 1,\ -1) \\ \mathbf{d'_R} &= (3,\ 1,\ -1/3), & \mathbf{u'_R} &= (3,\ 1,\ +2/3), & \phi &= (1,\ 2,\ +1/2) \\ & & Z' &= (1\,,1\,,0). \end{aligned} \tag{A.1}$$

References

[1] LHCb collaboration, *Test of lepton universality using $B^+ \to K^+\ell^+\ell^-$ decays*, *Phys. Rev. Lett.* **113** (2014) 151601 [arXiv:1406.6482] [INSPIRE].

[2] LHCb collaboration, *Test of lepton universality with $B^0 \to K^{*0}\ell^+\ell^-$ decays*, *JHEP* **08** (2017) 055 [arXiv:1705.05802] [INSPIRE].

JHEP03(2019)137

[3] LHCb collaboration, *Measurement of Form-Factor-Independent Observables in the Decay* $B^0 \to K^{*0}\mu^+\mu^-$, *Phys. Rev. Lett.* **111** (2013) 191801 [arXiv:1308.1707] [INSPIRE].

[4] LHCb collaboration, *Angular analysis of the* $B^0 \to K^{*0}\mu^+\mu^-$ *decay using* $3\,fb^{-1}$ *of integrated luminosity*, *JHEP* **02** (2016) 104 [arXiv:1512.04442] [INSPIRE].

[5] W. Altmannshofer and D.M. Straub, *New Physics in* $B \to K^*\mu\mu$*?*, *Eur. Phys. J.* **C 73** (2013) 2646 [arXiv:1308.1501] [INSPIRE].

[6] W. Altmannshofer and D.M. Straub, *New physics in* $b \to s$ *transitions after LHC run 1*, *Eur. Phys. J.* **C 75** (2015) 382 [arXiv:1411.3161] [INSPIRE].

[7] W. Altmannshofer, P. Stangl and D.M. Straub, *Interpreting Hints for Lepton Flavor Universality Violation*, *Phys. Rev.* **D 96** (2017) 055008 [arXiv:1704.05435] [INSPIRE].

[8] M. Ciuchini et al., *On Flavourful Easter eggs for New Physics hunger and Lepton Flavour Universality violation*, *Eur. Phys. J.* **C 77** (2017) 688 [arXiv:1704.05447] [INSPIRE].

[9] B. Capdevila, A. Crivellin, S. Descotes-Genon, J. Matias and J. Virto, *Patterns of New Physics in* $b \to s\ell^+\ell^-$ *transitions in the light of recent data*, *JHEP* **01** (2018) 093 [arXiv:1704.05340] [INSPIRE].

[10] L.-S. Geng, B. Grinstein, S. Jäger, J. Martin Camalich, X.-L. Ren and R.-X. Shi, *Towards the discovery of new physics with lepton-universality ratios of* $b \to s\ell\ell$ *decays*, *Phys. Rev.* **D 96** (2017) 093006 [arXiv:1704.05446] [INSPIRE].

[11] G. D'Amico et al., *Flavour anomalies after the* R_{K^*} *measurement*, *JHEP* **09** (2017) 010 [arXiv:1704.05438] [INSPIRE].

[12] S. Di Chiara et al., *Minimal flavor-changing* Z' *models and muon* $g-2$ *after the* R_{K^*} *measurement*, *Nucl. Phys.* **B 923** (2017) 245 [arXiv:1704.06200] [INSPIRE].

[13] R. Gauld, F. Goertz and U. Haisch, *On minimal* Z' *explanations of the* $B \to K^*\mu^+\mu^-$ *anomaly*, *Phys. Rev.* **D 89** (2014) 015005 [arXiv:1308.1959] [INSPIRE].

[14] A.J. Buras, F. De Fazio and J. Girrbach, *331 models facing new* $b \to s\mu^+\mu^-$ *data*, *JHEP* **02** (2014) 112 [arXiv:1311.6729] [INSPIRE].

[15] A.J. Buras and J. Girrbach, *Left-handed* Z' *and* Z *FCNC quark couplings facing new* $b \to s\mu^+\mu^-$ *data*, *JHEP* **12** (2013) 009 [arXiv:1309.2466] [INSPIRE].

[16] W. Altmannshofer, S. Gori, M. Pospelov and I. Yavin, *Quark flavor transitions in* $L_\mu - L_\tau$ *models*, *Phys. Rev.* **D 89** (2014) 095033 [arXiv:1403.1269] [INSPIRE].

[17] A.J. Buras, F. De Fazio and J. Girrbach-Noe, Z-Z' *mixing and* Z*-mediated FCNCs in* $\mathrm{SU}(3)_C \times \mathrm{SU}(3)_L \times \mathrm{U}(1)_X$ *models*, *JHEP* **08** (2014) 039 [arXiv:1405.3850] [INSPIRE].

[18] A. Crivellin, G. D'Ambrosio and J. Heeck, *Explaining* $h \to \mu^\pm\tau^\mp$, $B \to K^*\mu^+\mu^-$ *and* $B \to K\mu^+\mu^-/B \to Ke^+e^-$ *in a two-Higgs-doublet model with gauged* $L_\mu - L_\tau$, *Phys. Rev. Lett.* **114** (2015) 151801 [arXiv:1501.00993] [INSPIRE].

[19] A. Crivellin, G. D'Ambrosio and J. Heeck, *Addressing the LHC flavor anomalies with horizontal gauge symmetries*, *Phys. Rev.* **D 91** (2015) 075006 [arXiv:1503.03477] [INSPIRE].

[20] D. Aristizabal Sierra, F. Staub and A. Vicente, *Shedding light on the* $b \to s$ *anomalies with a dark sector*, *Phys. Rev.* **D 92** (2015) 015001 [arXiv:1503.06077] [INSPIRE].

[21] A. Crivellin, L. Hofer, J. Matias, U. Nierste, S. Pokorski and J. Rosiek, *Lepton-flavour violating* B *decays in generic* Z' *models*, *Phys. Rev.* **D 92** (2015) 054013 [arXiv:1504.07928] [INSPIRE].

JHEP03(2019)137

[22] A. Celis, J. Fuentes-Martin, M. Jung and H. Serodio, *Family nonuniversal Z' models with protected flavor-changing interactions*, *Phys. Rev.* **D 92** (2015) 015007 [arXiv:1505.03079] [INSPIRE].

[23] A. Greljo, G. Isidori and D. Marzocca, *On the breaking of Lepton Flavor Universality in B decays*, *JHEP* **07** (2015) 142 [arXiv:1506.01705] [INSPIRE].

[24] W. Altmannshofer and I. Yavin, *Predictions for lepton flavor universality violation in rare B decays in models with gauged $L_\mu - L_\tau$*, *Phys. Rev.* **D 92** (2015) 075022 [arXiv:1508.07009] [INSPIRE].

[25] B. Allanach, F.S. Queiroz, A. Strumia and S. Sun, *Z' models for the LHCb and $g-2$ muon anomalies*, *Phys. Rev.* **D 93** (2016) 055045 [*Erratum ibid.* **D 95** (2017) 119902] [arXiv:1511.07447] [INSPIRE].

[26] A. Falkowski, M. Nardecchia and R. Ziegler, *Lepton Flavor Non-Universality in B-meson Decays from a* U(2) *Flavor Model*, *JHEP* **11** (2015) 173 [arXiv:1509.01249] [INSPIRE].

[27] C.-W. Chiang, X.-G. He and G. Valencia, *Z' model for $b \to s\ell\bar{\ell}$ flavor anomalies*, *Phys. Rev.* **D 93** (2016) 074003 [arXiv:1601.07328] [INSPIRE].

[28] D. Bečirević, O. Sumensari and R. Zukanovich Funchal, *Lepton flavor violation in exclusive $b \to s$ decays*, *Eur. Phys. J.* **C 76** (2016) 134 [arXiv:1602.00881] [INSPIRE].

[29] S.M. Boucenna, A. Celis, J. Fuentes-Martin, A. Vicente and J. Virto, *Non-abelian gauge extensions for B-decay anomalies*, *Phys. Lett.* **B 760** (2016) 214 [arXiv:1604.03088] [INSPIRE].

[30] S.M. Boucenna, A. Celis, J. Fuentes-Martin, A. Vicente and J. Virto, *Phenomenology of an* $\mathrm{SU}(2) \times \mathrm{SU}(2) \times \mathrm{U}(1)$ *model with lepton-flavour non-universality*, *JHEP* **12** (2016) 059 [arXiv:1608.01349] [INSPIRE].

[31] P. Ko, Y. Omura, Y. Shigekami and C. Yu, *LHCb anomaly and B physics in flavored Z' models with flavored Higgs doublets*, *Phys. Rev.* **D 95** (2017) 115040 [arXiv:1702.08666] [INSPIRE].

[32] R. Alonso, P. Cox, C. Han and T.T. Yanagida, *Anomaly-free local horizontal symmetry and anomaly-full rare B-decays*, *Phys. Rev.* **D 96** (2017) 071701 [arXiv:1704.08158] [INSPIRE].

[33] R. Alonso, P. Cox, C. Han and T.T. Yanagida, *Flavoured $B-L$ local symmetry and anomalous rare B decays*, *Phys. Lett.* **B 774** (2017) 643 [arXiv:1705.03858] [INSPIRE].

[34] Y. Tang and Y.-L. Wu, *Flavor non-universal gauge interactions and anomalies in B-meson decays*, *Chin. Phys.* **C 42** (2018) 033104 [arXiv:1705.05643] [INSPIRE].

[35] J. Ellis, M. Fairbairn and P. Tunney, *Anomaly-Free Models for Flavour Anomalies*, *Eur. Phys. J.* **C 78** (2018) 238 [arXiv:1705.03447] [INSPIRE].

[36] C.-H. Chen and T. Nomura, *Penguin $b \to s\ell'^+\ell'^-$ and B-meson anomalies in a gauged $L_\mu - L_\tau$*, *Phys. Lett.* **B 777** (2018) 420 [arXiv:1707.03249] [INSPIRE].

[37] G. Faisel and J. Tandean, *Connecting $b \to s\ell\bar{\ell}$ anomalies to enhanced rare nonleptonic $\overline{B}{}^0_s$ decays in Z' model*, *JHEP* **02** (2018) 074 [arXiv:1710.11102] [INSPIRE].

[38] K. Fuyuto, H.-L. Li and J.-H. Yu, *Implications of hidden gauged* U(1) *model for B anomalies*, *Phys. Rev.* **D 97** (2018) 115003 [arXiv:1712.06736] [INSPIRE].

[39] L. Bian, H.M. Lee and C.B. Park, *B-meson anomalies and Higgs physics in flavored* $\mathrm{U}(1)'$ *model*, *Eur. Phys. J.* **C 78** (2018) 306 [arXiv:1711.08930] [INSPIRE].

JHEP03(2019)137

[40] M. Abdullah et al., *Bottom-quark fusion processes at the LHC for probing Z' models and B-meson decay anomalies*, *Phys. Rev.* **D 97** (2018) 075035 [arXiv:1707.07016] [INSPIRE].

[41] G.H. Duan, X. Fan, M. Frank, C. Han and J.M. Yang, *A minimal $U(1)'$ extension of MSSM in light of the B decay anomaly*, *Phys. Lett.* **B 789** (2019) 54 [arXiv:1808.04116] [INSPIRE].

[42] A. Crivellin, J. Fuentes-Martin, A. Greljo and G. Isidori, *Lepton Flavor Non-Universality in B decays from Dynamical Yukawas*, *Phys. Lett.* **B 766** (2017) 77 [arXiv:1611.02703] [INSPIRE].

[43] J.F. Kamenik, Y. Soreq and J. Zupan, *Lepton flavor universality violation without new sources of quark flavor violation*, *Phys. Rev.* **D 97** (2018) 035002 [arXiv:1704.06005] [INSPIRE].

[44] S.F. King, *$R_{K^{(*)}}$ and the origin of Yukawa couplings*, *JHEP* **09** (2018) 069 [arXiv:1806.06780] [INSPIRE].

[45] B.C. Allanach and J. Davighi, *Third Family Hypercharge Model for $R_{K^{(*)}}$ and Aspects of the Fermion Mass Problem*, *JHEP* **12** (2018) 075 [arXiv:1809.01158] [INSPIRE].

[46] B. Grinstein, S. Pokorski and G.G. Ross, *Lepton non-universality in B decays and fermion mass structure*, *JHEP* **12** (2018) 079 [arXiv:1809.01766] [INSPIRE].

[47] B.C. Allanach, B. Gripaios and T. You, *The case for future hadron colliders from $B \to K^{(*)}\mu^+\mu^-$ decays*, *JHEP* **03** (2018) 021 [arXiv:1710.06363] [INSPIRE].

[48] A. Greljo and D. Marzocca, *High-p_T dilepton tails and flavor physics*, *Eur. Phys. J.* **C 77** (2017) 548 [arXiv:1704.09015] [INSPIRE].

[49] S. Alioli, M. Farina, D. Pappadopulo and J.T. Ruderman, *Catching a New Force by the Tail*, *Phys. Rev. Lett.* **120** (2018) 101801 [arXiv:1712.02347] [INSPIRE].

[50] BaBar collaboration, *Evidence for an excess of $\bar{B} \to D^{(*)}\tau^-\bar{\nu}_\tau$ decays*, *Phys. Rev. Lett.* **109** (2012) 101802 [arXiv:1205.5442] [INSPIRE].

[51] BaBar collaboration, *Measurement of an Excess of $\bar{B} \to D^{(*)}\tau^-\bar{\nu}_\tau$ Decays and Implications for Charged Higgs Bosons*, *Phys. Rev.* **D 88** (2013) 072012 [arXiv:1303.0571] [INSPIRE].

[52] LHCb collaboration, *Measurement of the ratio of branching fractions $\mathcal{B}(\bar{B}^0 \to D^{*+}\tau^-\bar{\nu}_\tau)/\mathcal{B}(\bar{B}^0 \to D^{*+}\mu^-\bar{\nu}_\mu)$*, *Phys. Rev. Lett.* **115** (2015) 111803 [*Erratum ibid.* **115** (2015) 159901] [arXiv:1506.08614] [INSPIRE].

[53] Belle collaboration, *Measurement of the branching ratio of $\bar{B} \to D^{(*)}\tau^-\bar{\nu}_\tau$ relative to $\bar{B} \to D^{(*)}\ell^-\bar{\nu}_\ell$ decays with hadronic tagging at Belle*, *Phys. Rev.* **D 92** (2015) 072014 [arXiv:1507.03233] [INSPIRE].

[54] Belle collaboration, *Measurement of the branching ratio of $\bar{B}^0 \to D^{*+}\tau^-\bar{\nu}_\tau$ relative to $\bar{B}^0 \to D^{*+}\ell^-\bar{\nu}_\ell$ decays with a semileptonic tagging method*, *Phys. Rev.* **D 94** (2016) 072007 [arXiv:1607.07923] [INSPIRE].

[55] Belle collaboration, *Measurement of the τ lepton polarization and $R(D^*)$ in the decay $\bar{B} \to D^*\tau^-\bar{\nu}_\tau$*, *Phys. Rev. Lett.* **118** (2017) 211801 [arXiv:1612.00529] [INSPIRE].

[56] Belle collaboration, *Measurement of the τ lepton polarization and $R(D^*)$ in the decay $\bar{B} \to D^*\tau^-\bar{\nu}_\tau$ with one-prong hadronic τ decays at Belle*, *Phys. Rev.* **D 97** (2018) 012004 [arXiv:1709.00129] [INSPIRE].

[57] P. Arnan, L. Hofer, F. Mescia and A. Crivellin, *Loop effects of heavy new scalars and fermions in $b \to s\mu^+\mu^-$*, *JHEP* **04** (2017) 043 [arXiv:1608.07832] [INSPIRE].

JHEP03(2019)137

[58] Fermilab Lattice and MILC collaborations, *$B^0_{(s)}$-mixing matrix elements from lattice QCD for the Standard Model and beyond*, *Phys. Rev.* **D 93** (2016) 113016 [arXiv:1602.03560] [INSPIRE].

[59] M. Blanke and A.J. Buras, *Universal Unitarity Triangle 2016 and the tension between $\Delta M_{s,d}$ and ε_K in CMFV models*, *Eur. Phys. J.* **C 76** (2016) 197 [arXiv:1602.04020] [INSPIRE].

[60] W. Altmannshofer, S. Gori, S. Profumo and F.S. Queiroz, *Explaining dark matter and B decay anomalies with an $L_\mu - L_\tau$ model*, *JHEP* **12** (2016) 106 [arXiv:1609.04026] [INSPIRE].

[61] L. Di Luzio, M. Kirk and A. Lenz, *Updated B_s-mixing constraints on new physics models for $b \to s\ell^+\ell^-$ anomalies*, *Phys. Rev.* **D 97** (2018) 095035 [arXiv:1712.06572] [INSPIRE].

[62] A. Falkowski, M. González-Alonso and K. Mimouni, *Compilation of low-energy constraints on 4-fermion operators in the SMEFT*, *JHEP* **08** (2017) 123 [arXiv:1706.03783] [INSPIRE].

[63] A. Falkowski, S.F. King, E. Perdomo and M. Pierre, *Flavourful Z' portal for vector-like neutrino Dark Matter and $R_{K^{(*)}}$*, *JHEP* **08** (2018) 061 [arXiv:1803.04430] [INSPIRE].

[64] ATLAS collaboration, *Search for new high-mass phenomena in the dilepton final state using 36 fb^{-1} of proton-proton collision data at $\sqrt{s} = 13$ TeV with the ATLAS detector*, *JHEP* **10** (2017) 182 [arXiv:1707.02424] [INSPIRE].

[65] Y. Afik, J. Cohen, E. Gozani, E. Kajomovitz and Y. Rozen, *Establishing a Search for $b \to s\ell^+\ell^-$ Anomalies at the LHC*, *JHEP* **08** (2018) 056 [arXiv:1805.11402] [INSPIRE].

[66] M. Kohda, T. Modak and A. Soffer, *Identifying a Z' behind $b \to s\ell\ell$ anomalies at the LHC*, *Phys. Rev.* **D 97** (2018) 115019 [arXiv:1803.07492] [INSPIRE].

[67] R.D. Ball et al., *Parton distributions with LHC data*, *Nucl. Phys.* **B 867** (2013) 244 [arXiv:1207.1303] [INSPIRE].

[68] A. Buckley et al., *LHAPDF6: parton density access in the LHC precision era*, *Eur. Phys. J.* **C 75** (2015) 132 [arXiv:1412.7420] [INSPIRE].

[69] M. Lim, F. Maltoni, G. Ridolfi and M. Ubiali, *Anatomy of double heavy-quark initiated processes*, *JHEP* **09** (2016) 132 [arXiv:1605.09411] [INSPIRE].

[70] D.Yu. Bardin et al., *Z LINE SHAPE*, in *LEP Physics Workshop Geneva, Switzerland, February 20, 1989*, pp. 89–127, (1989).

[71] N.D. Christensen and C. Duhr, *FeynRules — Feynman rules made easy*, *Comput. Phys. Commun.* **180** (2009) 1614 [arXiv:0806.4194] [INSPIRE].

[72] C. Degrande, C. Duhr, B. Fuks, D. Grellscheid, O. Mattelaer and T. Reiter, *UFO — The Universal FeynRules Output*, *Comput. Phys. Commun.* **183** (2012) 1201 [arXiv:1108.2040] [INSPIRE].

[73] A. Alloul, N.D. Christensen, C. Degrande, C. Duhr and B. Fuks, *FeynRules 2.0 — A complete toolbox for tree-level phenomenology*, *Comput. Phys. Commun.* **185** (2014) 2250 [arXiv:1310.1921] [INSPIRE].

[74] J. Alwall et al., *The automated computation of tree-level and next-to-leading order differential cross sections and their matching to parton shower simulations*, *JHEP* **07** (2014) 079 [arXiv:1405.0301] [INSPIRE].

[75] T. Sjöstrand et al., *An Introduction to PYTHIA 8.2*, *Comput. Phys. Commun.* **191** (2015) 159 [arXiv:1410.3012] [INSPIRE].

JHEP03(2019)137

[76] M. Cacciari, G.P. Salam and G. Soyez, *FastJet User Manual*, *Eur. Phys. J.* **C 72** (2012) 1896 [arXiv:1111.6097] [INSPIRE].

[77] DELPHES 3 collaboration, *DELPHES 3, A modular framework for fast simulation of a generic collider experiment*, *JHEP* **02** (2014) 057 [arXiv:1307.6346] [INSPIRE].

[78] CMS collaboration, *Search for high-mass resonances in dilepton final states in proton-proton collisions at* $\sqrt{s} = 13$ *TeV*, *JHEP* **06** (2018) 120 [arXiv:1803.06292] [INSPIRE].

[79] CMS collaboration, *Search for narrow and broad dijet resonances in proton-proton collisions at* $\sqrt{s} = 13$ *TeV and constraints on dark matter mediators and other new particles*, *JHEP* **08** (2018) 130 [arXiv:1806.00843] [INSPIRE].

[80] ATLAS collaboration, *Search for new phenomena in dijet events using* $37\,fb^{-1}$ *of pp collision data collected at* $\sqrt{s} = 13$ *TeV with the ATLAS detector*, *Phys. Rev.* **D 96** (2017) 052004 [arXiv:1703.09127] [INSPIRE].

[81] J. Albrecht, F. Bernlochner, M. Kenzie, S. Reichert, D. Straub and A. Tully, *Future prospects for exploring present day anomalies in flavour physics measurements with Belle II and LHCb*, arXiv:1709.10308 [INSPIRE].

[82] BELLE II collaboration, *The Belle II Physics Book*, arXiv:1808.10567 [INSPIRE].

JHEP03(2019)137